Preprint number: XXXX-XXXX

Laplace expansion method for the calculation of the reduced width amplitudes

Yohei Chiba[1] and Masaaki Kimura[1,2]

[1]*Department of Physics, Hokkaido University, 060-0810 Sapporo, Japan*

[*]*E-mail: chiba@nucl.sci.hokudai.ac.jp*

[2]*Nuclear Reaction Data Centre, Hokkaido University, Sapporo 060-0810, Japan*

We derive the equations to calculate the reduced width amplitudes (RWA) of the different size clusters and deformed clusters without any approximation. These equations named Laplace expansion method are applicable to the nuclear models which uses the Gaussian wave packets. The advantage of the method is demonstrated by the numerical calculations of the $^{16}\mathrm{O} + \alpha$ and $^{24}\mathrm{Mg} + \alpha$ RWAs in $^{20}\mathrm{Ne}$ and $^{28}\mathrm{Si}$.

Subject Index xxxx, xxx

arXiv:1703.04569v1 [nucl-th] 14 Mar 2017

1 Introduction

In the excited states of light stable nuclei, it is well known that various cluster states appear as illustrated in Ikeda diagram [1]. They are composed of α, ^{12}C and ^{16}O clusters which are tightly bound and stable compared to the neighboring nuclei. In these decades, the study of nuclear clustering is extended to unstable nuclei where novel types of clustering were found. The molecular-orbit and atomic-orbit states in Be isotopes [2–11] are the representative of such novel types of clustering. In contrast to the clustering of light stable nuclei, they are composed of ^{6}He and ^{8}He which are weakly bound and unstable. Since the definition of the cluster is extended from the ordinary one, we need a good measure for these non-conventional clustering.

The reduced width amplitude is one of such measures for the clustering. It is the cluster formation probability at a given inter-cluster distance, and hence, it is regarded as a direct evidence of the clustering. By the R-matrix theory [12], the RWA is derived from the width of the cluster states which are experimentally determined by the measurement of the cluster decay lifetime, the resonant scattering and the transfer reactions. Therefore, numerous experiments have been conducted to determine the RWA and to identify various clusters. A variety of cluster states in light p-sd-shell nuclei illustrated in the Ikeda diagram have been identified from their large decay widths and RWAs [13–17]. Several clusters in heavier pf-nuclei were established in 1990's when the measurements of the RWAs played an essential role to identify the α cluster states of ^{40}Ca and ^{44}Ti [18–28]. More recently, the α decay property has been used in combination with the isoscalar monopole and dipole transitions to identify the gas-like α cluster states [29–35] and various clusters in sd-shell nuclei [36–41]. The importance of the RWA for the study of exotic clustering in neutron-rich nuclei must also be emphasized. It was an important observable to identify the molecular clustering in Be isotopes [7–10]. More recently, the cluster states in ^{18}O and ^{22}Ne [42–53] and linear-chain states in ^{14,16}C [54–67] are discussed from their α decays and RWAs. Thus, the comparison of the measured RWA with the theoretical ones is indispensable to establish the cluster formation.

However, in the theoretical studies, the calculation of RWA for general cluster systems is not easy due to the antisymmetrization of nucleons belonging to the different clusters. To simplify the treatment of the antisymmetrization, the ordinary methods for RWA calculation [68–73] often approximate the cluster wave functions with the $SU(3)$ shell model wave functions [74, 75] having the common oscillator parameters (the same size of clusters). Unfortunately, this approximation limits the applicability of the methods. They are inaccurate when applied to the unequal size clusters and the clusters which cannot be approximated

by a single $SU(3)$ shell model wave function. Typical examples of this may be the $^{16}\mathrm{O}+\alpha$ and $^{6}\mathrm{He}+\alpha$ clusters, *i.e.* the size of these clusters are different and a halo nucleus ^{6}He cannot be described by a single $SU(3)$ shell model wave function. Furthermore, to calculate the RWA of deformed clusters, the ordinary methods demand much computational time because of the multiple angular momentum projections. Although an approximate method proposed by Kanada-En'yo *et al.* [76] reduced the computational cost to some extent, the development of an alternative method for RWA calculation is highly desirable and in need.

For this purpose, we present a new method for the RWA calculation. We derive the equations which can calculate the RWA of the different size clusters and deformed clusters without any approximation. These equations named Laplace expansion method are applicable to nuclear models which uses the Gaussian wave packets such as antisymmetrized molecular dynamics (AMD) [77–79]. This paper is organized as follows. In the next section, we derive the equations of the Laplace expansion method. We also discuss the advantages and disadvantages of the method compared to the ordinary method. In the section 3, we show the numerical results of the $^{16}\mathrm{O}+\alpha$ and $^{24}\mathrm{Mg}+\alpha$ RWAs as the examples of the unequal size clusters and deformed clusters. In the final section, we summarize the present work.

2 Laplace expansion method for RWA calculation

In this section, we outline a new method to calculate the RWA which utilizes the Laplace expansion of the matrix determinant. We first introduce the AMD wave function. Then, by using the Laplace expansion, we show that the AMD wave function of A-body system can be decomposed into those of the subsystems with masses C_1 and C_2. With this expansion, we derive the equations to calculate the RWA which we call Laplace expansion method. We also compare the Laplace expansion method with ordinary one to discuss its advantages and disadvantages.

2.1 Wave function of antisymmetrized molecular dynamics

The wave function of AMD for A-body system is a Slater determinant of the Gaussian wave packets describing nucleons.

$$\Psi_A^{AMD} = \frac{1}{\sqrt{C_1!}} \begin{vmatrix} \langle \boldsymbol{r}_1|\psi_1\rangle & \dots & \langle \boldsymbol{r}_1|\psi_A\rangle \\ \vdots & \ddots & \vdots \\ \langle \boldsymbol{r}_A|\psi_1\rangle & \dots & \langle \boldsymbol{r}_A|\psi_A\rangle \end{vmatrix}, \tag{1}$$

$$\langle \boldsymbol{r}|\psi_i\rangle = \left(\frac{|2M|}{\pi^3}\right)^{1/4} \exp\left\{-(\boldsymbol{r}-\boldsymbol{Z}_i)^T M(\boldsymbol{r}-\boldsymbol{Z}_i)\right\}(\alpha_i\chi_\uparrow + \beta_i\chi_\downarrow)\eta_i, \tag{2}$$

where the Gaussian centroids $\boldsymbol{Z}_i$ are the complex valued three dimensional vector, and the spin directions are parameterized by the complex variables α_i and β_i. The isospin part η_i is fixed to either of proton or neutron. Each nucleon wave packet has these independent variables. To discuss the general case, we assume the use of the deformed Gaussian wave packets [73], and hence, M denote a symmetric positive-definite 3×3 matrix.

If the width matrix M is common for all nucleon wave packets, the AMD wave function can be straightforwardly decomposed into the internal wave function Ψ_A^{int} and the center-of-mass wave function Ψ_A^{cm},

$$\Psi_A^{AMD} = \Psi_A^{int}\Psi_A^{cm}, \tag{3}$$

$$\Psi_A^{cm} = \left(\frac{|2AM|}{\pi^3}\right)^{1/4} \exp\left\{-A(\boldsymbol{R}-\boldsymbol{Z})^T M(\boldsymbol{R}-\boldsymbol{Z})\right\}, \tag{4}$$

$$\boldsymbol{R} = \frac{1}{A}\sum_{i=1}^{A}\boldsymbol{r}_i, \quad \boldsymbol{Z} = \frac{1}{A}\sum_{i=1}^{A}\boldsymbol{Z}_i. \tag{5}$$

This simple but important decomposition is repeatedly used in the Laplace expansion method. Without loss of generality, we assume that $\boldsymbol{Z}_i$ satisfy the relation $\sum_{i=1}^{A}\boldsymbol{Z}_i = 0$.

The AMD wave function given by Eq. (1) is not an eigenstate of the parity and angular momentum. Therefore, the parity and angular momentum projections are usually performed.

$$\Psi_{MKA}^{J\pi} = \frac{1}{\sqrt{\mathcal{N}_K^{J\pi}}}\hat{P}_{MK}^J\hat{P}^\pi\Psi_A^{int}, \tag{6}$$

$$\mathcal{N}_K^{J\pi} = \left\langle \Psi_A^{int} \middle| \hat{P}_{KK}^J\hat{P}^\pi \middle| \Psi_A^{int} \right\rangle, \tag{7}$$

$$\hat{P}_{MK}^J = \int d\Omega D_{MK}^{J*}(\Omega)\hat{R}(\Omega), \quad \hat{P}^\pi = \frac{1+\pi\hat{P}_r}{2}, \quad \pi = \pm, \tag{8}$$

where $\hat{P}_{MK}^J$ and $\hat{P}^\pi$ are the angular momentum and parity projectors. $D_{MK}^J(\Omega)$ and $\hat{R}(\Omega)$ are the Wigner D function and rotation operator dependent on the Euler angles Ω. $\hat{P}_r$ is the parity operator.

In addition to the projection, in nuclear structure studies, the parity and angular momentum projected AMD wave functions are superposed to take the effects of the configuration

mixing and the shape fluctuation into account (generator coordinate method; GCM).

$$\Psi^{J\pi}_{MA} = \sum_{s=1}^{s_{max}} \sum_{K=-J}^{J} c_{sK} \frac{1}{\sqrt{\mathcal{N}^{J\pi}_{K}(s)}} \hat{P}^{J}_{MK} \hat{P}^{\pi} \Psi^{int}_{A}(s) = \sum_{s=1}^{s_{max}} \sum_{K=-J}^{J} c_{sK} \Psi^{J\pi}_{MKA}(s), \quad (9)$$

$$\Psi^{J\pi}_{MKA}(s) = \frac{1}{\sqrt{\mathcal{N}^{J\pi}_{K}(s)}} \hat{P}^{J}_{MK} \hat{P}^{\pi} \Psi^{int}_{A}(s), \quad (10)$$

$$\mathcal{N}^{J\pi}_{K}(s) = \left\langle \Psi^{int}_{A}(s) \middle| \hat{P}^{J}_{KK} \hat{P}^{\pi} \middle| \Psi^{int}_{A}(s) \right\rangle, \quad (11)$$

where s is the index for the internal wave functions and c_{sK} is the coefficient of the superposition. Hereafter, we denote the wave functions given by Eq. (1), (6) and (9) as "AMD wave function", "projected AMD wave function" and "GCM wave function", respectively.

It must be noted that the following discussion and the Laplace expansion method are also applicable to the Brink-Bloch wave function [80] and $SU(3)$ shell model wave function (harmonic oscillator wave function without the spin-orbit splitting), because the AMD wave function includes the Brink-Bloch wave function and $SU(3)$ shell model wave function as its spacial cases. When the centroid of the wave packets are common for the quartet of $n\uparrow$, $n\downarrow$, $p\uparrow$ and $p\downarrow$, the AMD wave function is equal to the Brink-Bloch wave function for $N\alpha$ systems. At the limit of the $\boldsymbol{Z}_i \to 0$ the AMD wave function is equal to the $SU(3)$ shell model wave function.

2.2 Laplace expansion of the AMD wave function

The Laplace expansion of the determinant of an $A \times A$ matrix B is given as,

$$|B| = \sum_{1 \le i_1 < \cdots < i_{C_1} \le A} P(i_1, \ldots, i_{C_1}) |B(i_1, \ldots, i_{C_1})| |B(i_{C_1+1}, \ldots, i_A)|, \quad (12)$$

where the summation runs over all possible combinations of indices $i_1, \ldots, i_{C_1}$. The phase factor $P(i_1, \ldots, i_{C_1})$ is defined as

$$P(i_1, \ldots, i_{C_1}) = (-)^{C_1(C_1+1)/2 + \sum_{s=1}^{C_1} i_s}. \quad (13)$$

$|B(i_1, \ldots, i_{C_1})|$ is the determinant of the $C_1 \times C_1$ matrix composed from the $1, ..., C_1$th rows and the $i_1, \ldots, i_{C_1}$th columns of the matrix B

$$|B(i_1, \ldots, i_{C_1})| = \begin{vmatrix} B_{1i_1} & \ldots & B_{1i_{C_1}} \\ \vdots & \ddots & \vdots \\ B_{C_1 i_1} & \ldots & B_{C_1 i_{C_1}} \end{vmatrix}, \quad (14)$$

and $|B(i_{C_1+1}, \dots i_A)|$ is the determinant of the $C_2 \times C_2$ matrix ($C_1 + C_2 = A$) formed by removing the $1, \dots, C_1$th rows and the $i_1, \dots, i_{C_1}$th columns from B,

$$|B(i_{C_1+1}, \dots, i_A)| = \begin{vmatrix} B_{C_1+1,i_{C_1+1}} & \dots & B_{C_1+1,i_A} \\ \vdots & \ddots & \vdots \\ B_{A,i_{C_1+1}} & \dots & B_{A,i_A} \end{vmatrix}, \tag{15}$$

where $i_{C_1+1}, ..., i_A$ denote the column indices other than $i_1, ..., i_{C_1}$ and satisfy the relation $1 \le i_{C_1+1} < ... < i_A \le A$.

Applying the Laplace expansion to the A-body AMD wave function given by Eq. (1), we obtain the decomposition of the AMD wave function,

$$\Psi_A^{AMD} = \sqrt{\frac{C_1!C_2!}{A!}} \sum_{1 \le i_1 < \dots < i_{C_1} \le A} P(i_1, \dots, i_{C_1}) \Psi_{C_1}^{AMD}(i_1, \dots, i_{C_1}) \Psi_{C_2}^{AMD}(i_{C_1+1}, \dots, i_A). \tag{16}$$

Here, $\Psi_{C_1}^{AMD}(i_1, \dots, i_{C_1})$ and $\Psi_{C_2}^{AMD}(i_{C_1+1}, \dots, i_A)$ are the AMD wave functions for the subsystems with masses C_1 and C_2 which are defined as

$$\Psi_{C_1}^{AMD}(i_1, \dots, i_{C_1}) = \frac{1}{\sqrt{C_1!}} \begin{vmatrix} \langle \boldsymbol{r}_1 | \psi_{i_1} \rangle & \dots & \langle \boldsymbol{r}_1 | \psi_{i_{C_1}} \rangle \\ \vdots & \ddots & \vdots \\ \langle \boldsymbol{r}_{C_1} | \psi_{i_1} \rangle & \dots & \langle \boldsymbol{r}_{C_1} | \psi_{i_{C_1}} \rangle \end{vmatrix}, \tag{17}$$

$$\Psi_{C_2}^{AMD}(i_{C_1+1}, , \dots, i_A) = \frac{1}{\sqrt{C_2!}} \begin{vmatrix} \langle \boldsymbol{r}_{C_1+1} | \psi_{i_{C_1+1}} \rangle & \dots & \langle \boldsymbol{r}_{C_1+1} | \psi_{i_A} \rangle \\ \vdots & \ddots & \vdots \\ \langle \boldsymbol{r}_A | \psi_{i_{C_1+1}} \rangle & \dots & \langle \boldsymbol{r}_A | \psi_{i_A} \rangle \end{vmatrix}. \tag{18}$$

Since the internal and the center-of-mass wave functions are analytically separable as shown in Eq. (3), the product of the AMD wave functions in the right hand side of Eq. (16) is equal to a product of the internal and center-of-mass wave functions of the subsystems,

$$\Psi_{C_1}^{AMD} \Psi_{C_2}^{AMD} = \Psi_{C_1}^{cm} \Psi_{C_2}^{cm} \Psi_{C_1}^{int} \Psi_{C_2}^{int}, \tag{19}$$

$$\Psi_{C_1}^{cm} = \left(\frac{|2C_1 M|}{\pi^3} \right)^{1/4} \exp\left\{ -C_1 (\boldsymbol{R}_{C_1} - \boldsymbol{Z}_{C_1})^T M (\boldsymbol{R}_{C_1} - \boldsymbol{Z}_{C_1}) \right\}, \tag{20}$$

$$\Psi_{C_2}^{cm} = \left(\frac{|2C_2 M|}{\pi^3} \right)^{1/4} \exp\left\{ -C_2 (\boldsymbol{R}_{C_2} - \boldsymbol{Z}_{C_2})^T M (\boldsymbol{R}_{C_2} - \boldsymbol{Z}_{C_2}) \right\}, \tag{21}$$

$$\boldsymbol{R}_{C_1} = \frac{1}{C_1} \sum_{i=1}^{C_1} \boldsymbol{r}_i, \quad \boldsymbol{R}_{C_2} = \frac{1}{C_1} \sum_{i=C_1+1}^{A} \boldsymbol{r}_i, \tag{22}$$

$$\boldsymbol{Z}_{C_1} = \frac{1}{C_1} \sum_{i \in \{i_1, \dots, i_{C_1}\}} \boldsymbol{Z}_i, \quad \boldsymbol{Z}_{C_2} = \frac{1}{C_2} \sum_{i \in \{i_{C_1+1}, \dots, i_A\}} \boldsymbol{Z}_i, \tag{23}$$

where we suppressed the indices $i_1, ..., i_A$ for simplicity. $\boldsymbol{R}_{C_1}$ and $\boldsymbol{R}_{C_2}$ denote the center-of-mass coordinates of the subsystems. Then, we rewrite the product of the center-of-mass wave functions of clusters to the product of the center-of-mass wave function of A-body system Ψ^{cm}_A and the relative wave function between the subsystems $\chi(\boldsymbol{r})$.

$$\Psi^{cm}_{C_1}\Psi^{cm}_{C_2} = \Psi^{cm}_A \chi(\boldsymbol{r}), \tag{24}$$

$$\chi(\boldsymbol{r}) = \left(\frac{|2\Gamma|}{\pi^3}\right)^{1/4} \exp\left\{-(\boldsymbol{r}-\boldsymbol{z})^T\Gamma(\boldsymbol{r}-\boldsymbol{z})\right\}, \tag{25}$$

$$\boldsymbol{r} = \boldsymbol{R}_{C_1} - \boldsymbol{R}_{C_2}, \quad \boldsymbol{z} = \boldsymbol{Z}_{C_1} - \boldsymbol{Z}_{C_2}, \quad \Gamma = \frac{C_1C_2}{A}M. \tag{26}$$

As a result, the product of the AMD wave functions is transformed as follows,

$$\Psi^{AMD}_{C_1}(i_1, ..., i_{C_1})\Psi^{AMD}_{C_2}(i_{C_1+1}, ..., i_A) = \Psi^{cm}_A \chi(\boldsymbol{r}; i_1, ..., i_A)\Psi^{int}_{C_1}(i_1, ..., i_{C_1})\Psi^{int}_{C_2}(i_{C_1+1}, ..., i_A). \tag{27}$$

Note that Ψ^{cm}_A is independent of the choice of $i_1, \ldots, i_{C_1}$. Substituting Eq. (27) into Eq. (16), and removing the center-of-mass wave function, we obtain a decomposition of A-body internal wave function into two subsystems with masses C_1 and C_2.

$$\Psi^{int}_A = \sqrt{\frac{C_1!C_2!}{A!}} \sum_{1\le i_1<\cdots<i_{C_1}\le A} P(i_1, \ldots, i_{C_1})\chi(\boldsymbol{r}; i_1, \ldots i_A)\Psi^{int}_{C_1}(i_1, \ldots, i_{C_1})\Psi^{int}_{C_2}(i_{C_1+1}, \ldots, i_A). \tag{28}$$

It is noted that the Laplace expansion can be applied recursively, and hence, the decompositions of the A-body wave function into three and more subsystems are also straightforward.

2.3 Calculation of the RWA using Laplace expansion

Using Laplace expansion of AMD wave function, we can calculate RWA of the $C_1 + C_2$ cluster system without any approximation. First, we discuss the RWA of a single projected AMD wave function, and the extension to the GCM wave function is discussed later.

The RWA for two-body cluster system is defined as the overlap amplitude between the A-body wave function $\Psi^{J\pi}_{MA}$ and the reference state composed of the clusters with masses C_1 and C_2,

$$y^{J\pi}_{j_1\pi_1 j_2\pi_2 j_{12} l}(a) = \sqrt{\frac{A!}{(1+\delta_{C_1C_2})C_1!C_2!}} \left\langle \frac{\delta(r-a)}{r^2}\left[Y_l(\hat{r})\left[\Phi^{j_1\pi_1}_{C_1}\Phi^{j_2\pi_2}_{C_2}\right]_{j_{12}}\right]_{JM} \middle| \Psi^{J\pi}_{MA}\right\rangle, \tag{29}$$

where $\Phi^{j_1\pi_1}_{C_1}$ and $\Phi^{j_2\pi_2}_{C_2}$ are the wave functions of clusters C_1 and C_2. Their spins j_1 and j_2 are coupled to j_{12}, and j_{12} is coupled to orbital angular momentum l of the inter-cluster

motion to yield the total spin-parity J^π. Therefore, π_1, π_2 and l must satisfy the relation $\pi = \pi_1\pi_2(-)^l$. We assume that the wave functions $\Psi^{J\pi}_{MA}$, $\Phi^{j_1\pi_1}_{C_1}$ and $\Phi^{j_2\pi_2}_{C_2}$ are antisymmetrized and normalized.

With this definition, by substituting Eq. (6) into (29), the RWA of a projected AMD wave function reads,

$$
\begin{aligned}
y^{J\pi}_{j_1\pi_1 j_2\pi_2 j_{12} l}(a) =& \sqrt{\frac{A!}{(1+\delta_{C_1C_2})C_1!C_2!}} \left\langle \frac{\delta(r-a)}{r^2} \left[Y_l(\hat{r}) \left[\Phi^{j_1\pi_1}_{C_1} \Phi^{j_2\pi_2}_{C_2} \right]_{j_{12}} \right]_{JM} \middle| \Psi^{J\pi}_{MKA} \right\rangle \\
=& \frac{1}{\sqrt{\mathcal{N}^{J\pi}_K}} \sqrt{\frac{A!}{(1+\delta_{C_1C_2})C_1!C_2!}} \left\langle \frac{\delta(r-a)}{r^2} \hat{P}^J_{KM} \left[Y_l(\hat{r}) \left[\Phi^{j_1\pi_1}_{C_1} \Phi^{j_2\pi_2}_{C_2} \right]_{j_{12}} \right]_{JM} \middle| \Psi^{int}_A \right\rangle \\
=& \frac{1}{\sqrt{\mathcal{N}^{J\pi}_K}} \sqrt{\frac{A!}{(1+\delta_{C_1C_2})C_1!C_2!}} \left\langle \frac{\delta(r-a)}{r^2} \left[Y_l(\hat{r}) \left[\Phi^{j_1\pi_1}_{C_1} \Phi^{j_2\pi_2}_{C_2} \right]_{j_{12}} \right]_{JK} \middle| \Psi^{int}_A \right\rangle \\
=& \frac{1}{\sqrt{\mathcal{N}^{J\pi}_K}} \sqrt{\frac{A!}{(1+\delta_{C_1C_2})C_1!C_2!}} \sum_{m_{12}m_l m_1 m_2} C^{JK}_{lm_l j_{12}m_{12}} C^{j_{12}m_{12}}_{j_1 m_1 j_2 m_2} \\
& \times \left\langle \frac{\delta(r-a)}{r^2} Y_{lm_l}(\hat{r}) \Phi^{j_1\pi_1}_{m_1C_1} \Phi^{j_2\pi_2}_{m_2C_2} \middle| \Psi^{int}_A \right\rangle ,
\end{aligned}
\tag{30}
$$

where we used the relation $\pi = \pi_1\pi_2(-)^l$ and the properties of the angular momentum projector $(\hat{P}^J_{MK})^\dagger = \hat{P}^J_{KM}$ and $\hat{P}^{J\pi}_{KM}|JM\rangle = |JK\rangle$. $C^{JM}_{j_1m_1j_2m_2}$ denotes the Clebsch-Gordan coefficient. By using the Laplace expansion of Ψ^{int}_A given by Eq. (28), the braket in the right hand side of Eq. (30) is written as

$$
\begin{aligned}
& \left\langle \frac{\delta(r-a)}{r^2} Y_{lm_l}(\hat{r}) \Phi^{j_1\pi_1}_{m_1C_1} \Phi^{j_2\pi_2}_{m_2C_2} \middle| \Psi^{int}_A \right\rangle = \sqrt{\frac{C_1!C_2!}{A!}} \sum_{1\le i_1<\ldots<i_{C_1}\le A} P(i_1,\ldots,i_{C_1}) \\
& \times \left\langle \frac{\delta(r-a)}{r^2} Y_{lm_l}(\hat{r}) \Phi^{j_1\pi_1}_{m_1C_1} \Phi^{j_2\pi_2}_{m_2C_2} \middle| \chi(\boldsymbol{r}; i_1,\ldots,i_A) \Psi^{int}_{C_1}(i_1,\ldots,i_{C_1}) \Psi^{int}_{C_2}(i_{C_1+1},\ldots,i_A) \right\rangle .
\end{aligned}
\tag{31}
$$

Note that the braket in the last line has no antisymmetrizer with respect to the nucleons belonging to different subsystems. Therefore, it is equal to the product of the overlaps between the relative wave functions and between the subsystems.

$$
\begin{aligned}
& \left\langle \frac{\delta(r-a)}{r^2} Y_{lm_l}(\hat{r}) \Phi^{j_1\pi_1}_{m_1C_1} \Phi^{j_2\pi_2}_{m_2C_2} \middle| \chi(\boldsymbol{r}; i_1,\ldots,i_A) \Psi^{int}_{C_1}(i_1,\ldots,i_{C_1}) \Psi^{int}_{C_2}(i_{C_1+1},\ldots,i_A) \right\rangle \\
& = \left\langle \frac{\delta(r-a)}{r^2} Y_{lm_l}(\hat{r}) \middle| \chi(\boldsymbol{r}; i_1,\ldots,i_A) \right\rangle \left\langle \Phi^{j_1\pi_1}_{m_1C_1} | \Psi^{int}_{C_1}(i_1,\ldots,i_{C_1}) \right\rangle \left\langle \Phi^{j_2\pi_2}_{m_2C_2} | \Psi^{int}_{C_2}(i_{C_1+1},\ldots,i_A) \right\rangle .
\end{aligned}
\tag{32}
$$

Substituting Eqs. (31) and (32) to Eq. (30), we obtain the RWA of a projected AMD wave function.

$$y^{J\pi}_{j_1\pi_1 j_2\pi_2 j_{12} l}(a) = \frac{1}{\sqrt{\mathcal{N}^{J\pi}_K(1+\delta_{C_1C_2})}} \sum_{1\le i_1<\ldots<i_A\le A} P(i_1,\ldots,i_{C_1}) \times \left[\chi_l(a;i_1,\ldots,i_A)\left[N^{j_1\pi_1}(i_1,\ldots,i_{C_1})N^{j_2\pi_2}(i_{C_1+1},\ldots i_A)\right]_{j_{12}}\right]_{JK}, \tag{33}$$

with the definitions of the overlaps,

$$\chi_{lm_l}(a;i_1,\ldots,i_A) = \left\langle \frac{\delta(r-a)}{r^2}Y_{lm_l}(\hat{r}) \,\middle|\, \chi(\boldsymbol{r};i_1,\ldots,i_A)\right\rangle, \tag{34}$$

$$N^{j_1\pi_1}_{m_1}(i_1,\ldots,i_{C_1}) = \langle \Phi^{j_1\pi_1}_{m_1C_1} | \Psi^{int}_{C_1}(i_1,\ldots,i_{C_1})\rangle, \tag{35}$$

$$N^{j_2\pi_2}_{m_2}(i_{C1+1},\ldots,i_A) = \langle \Phi^{j_2\pi_2}_{m_2C_2} | \Psi^{int}_{C_2}(i_{C_1+1},\ldots,i_A)\rangle. \tag{36}$$

Thus, the RWA is obtained by calculating the overlaps defined by Eqs. (34), (35) and (36) which are easily calculated as explained in the appendix A.

The extension of the method to the GCM wave function is straightforward. Substituting Eq. (9) to Eq. (29), one easily obtains the RWA of GCM wave function as follows.

$$y^{J\pi}_{j_1\pi_1 j_2\pi_2 j_{12} l}(a) = \sum_{s=1}^{s_{max}}\sum_{K=-J}^{J} c_{sK} y^{J\pi}_{j_1\pi_1 j_2\pi_2 j_{12} l}(a;sK) \tag{37}$$

$$y^{J\pi}_{j_1\pi_1 j_2\pi_2 j_{12} l}(a;sK) = \sqrt{\frac{A!}{C_1!C_2!}}\left\langle \frac{\delta(r-a)}{r^2}\left[Y_l(\hat{r})\left[\Phi^{j_1\pi_1}_{C_1}\Phi^{j_2\pi_2}_{C_2}\right]_{j_{12}}\right]_{JM} \,\middle|\, \Psi^{J\pi}_{MKA}(s)\right\rangle. \tag{38}$$

Thus, the RWA of the GCM wave function is the superposition of the RWAs of the projected AMD wave functions defined by Eq. (38) which are calculated by using Eq. (33) for every $\Psi^{J\pi}_{MKA}(s)$. In a same way, when the reference wave function $\Phi^{j_1\pi_1}_{m_1C_1}$ is a GCM wave function, the overlap $N^{j_1\pi_1}_{m_1}(i_1,...,i_{C_1})$ is a sum of the overlaps of the projected AMD wave functions.

2.4 Advantages of the Laplace expansion method

It may be worthwhile to compare the Laplace expansion method with an ordinary method [70–73] which is often used in the cluster models and AMD to see its advantages and disadvantages. The ordinary method uses a set of the projected Brink-Bloch type wave functions

defined as

$$\Phi^{J\pi}_{j_1\pi_1 j_2\pi_2 j_{12} l}(S_p) = \frac{2l+1}{2J+1} \sum_{m_{12}m_1m_2} C^{Jm_{12}}_{l0j_{12}m_{12}} \hat{P}^J_{Mm_{12}} C^{j_{12}m_{12}}_{j_1m_1j_2m_2} \Phi^{BB}_{j_1\pi_1 m_1 j_2\pi_2 m_2}(S_p), \tag{39}$$

$$\Phi^{BB}_{j_1\pi_1 m_1 j_2\pi_2 m_2}(S_p) = \sqrt{\frac{C_1!C_2!}{A!}} \mathcal{A}\left\{ \hat{P}^{j_1}_{m_1k_1} \hat{P}^{\pi_1} \Phi_{C_1}\left(-\frac{C_2}{A}\boldsymbol{S}_p\right) \hat{P}^{j_2}_{m_2k_2} \hat{P}^{\pi_2} \Phi_{C_2}\left(\frac{C_1}{A}\boldsymbol{S}_p\right)\right\}, \tag{40}$$

$$\boldsymbol{S}_p = (0,0,S_p). \tag{41}$$

$\Phi_{C_1}\left(-C_2/A\boldsymbol{S}_p\right)$ and $\Phi_{C_2}\left(C_1/A\boldsymbol{S}_p\right)$ are the wave functions for clusters with masses C_1 and C_2 with their center-of-mass wave functions, and placed with the inter-cluster distance S_p. The inter-cluster distance S_p is discretized, for example, as

$$S_p = p\Delta S, \quad p = 1, ..., p_{max}. \tag{42}$$

The following three conditions are often required to reduce the computational cost.

- Φ_{C_1} and Φ_{C_2} are the $SU(3)$ shell model wave functions without particle-hole excitations.
- The oscillator parameters of Φ_{C_1} and Φ_{C_2} are the same value, $\hbar\omega = 2\hbar^2\nu/m$
- Φ_{C_1} and Φ_{C_2} are the eigenstates of the principal quantum number $\hat{N}$

With these conditions are satisfied, the RWA is given as follows,

$$y^{J\pi}_{j_1\pi_1 j_2\pi_2 j_{12} l}(a) = \frac{1}{\sqrt{1+\delta_{C_1C_2}}} \sum_N \mu_{Nl} e_N R_{Nl}(r), \tag{43}$$

$$\mu_{Nl} = \left\langle R_{Nl}(r)\left[Y_l(\hat{r})\left[\Phi^{j_1\pi_1}_{C_1}\Phi^{j_2\pi_2}_{C_2}\right]_{j_{12}}\right]_J \middle| \mathcal{A}\left\{R_{Nl}(r)\left[Y_l(\hat{r})\left[\Phi^{j_1\pi_1}_{C_1}\Phi^{j_2\pi_2}_{C_2}\right]_{j_{12}}\right]_J\right\}\right\rangle, \tag{44}$$

$$e_{Nl} = (-)^{(N-l)/2}\sqrt{\frac{(2l+1)}{(N-l)!!(N+l+1)!!}} \sum_{pq} \frac{(\nu S_p^2)^{N/2}}{\sqrt{N!}} e^{-\nu S_p^2/2} B^{-1}_{pq} \left\langle \Phi^{J\pi}_{j_1\pi_1 j_2\pi_2 j_{12} l}(S_q) | \Psi^{J\pi}_{MA} \right\rangle, \tag{45}$$

$$B_{pq} = \left\langle \Phi^{J\pi}_{j_1\pi_1 j_2\pi_2 j_{12} l}(S_p) | \Phi^{J\pi}_{j_1\pi_1 j_2\pi_2 j_{12} l}(S_q) \right\rangle. \tag{46}$$

Here $R_{Nl}(r)$ is the radial wave function of harmonic oscillator (HO). The derivation of these equations is explained in the appendix B and the Refs. [70–73]. From these equations, we can see several advantages of the Laplace expansion method listed below.

(1) The size of the Gaussian wave packets describing clusters C_1 and C_2 in the reference state can be different in the Laplace expansion method. This is an advantage when we calculate the RWA of the different size clusters such as $^{16}\mathrm{O} + \alpha$ and

$^{40}\mathrm{Ca} + \alpha$ [81].

On the other hand, in the ordinary method, they must be equal to analytically separate the center-of-mass and relative wave functions as explained in the appendix B.

(2) The deformed Gaussian wave packets can be used to describe the clusters C_1 and C_2 in the reference state. Therefore, the Laplace expansion method can easily calculate the RWA of deformed clusters such as $^{10}\mathrm{Be} + \alpha$ and $^{24}\mathrm{Mg} + \alpha$ without any approximation.

On the other hand, for the analytical separation of the center-of-mass and the relative wave functions, ordinary method uses spherical Gaussian. For example, in Ref. [64, 67], ^{10}Be wave function was approximated by the spherical Gaussian to estimate the $^{10}\mathrm{Be} + \alpha$ RWA.

(3) The angular momentum projection of the cluster wave functions can be done with much reduced computational cost. This is another advantage when we calculate the RWA of the deformed clusters.

When the intrinsic wave function of clusters Φ_{C_1} and Φ_{C_2} are not the eigenstate of the angular momentum, we need to perform the angular momentum projection of each cluster. In the ordinary method, we need to calculate Eqs. (45) and (46), which contain three and five angular momentum projectors and demand huge computational cost. Therefore, the approximation is often applied [64, 67]. However, in the case of the Laplace expansion method, we only need to calculate Eqs. (35) and (36) which contain only one angular momentum projector.

(4) The GCM wave function can be used as the wave functions of clusters. Therefore, the Laplace expansion method can treat various clusters which cannot be described by a single AMD wave function. A typical example is ^{6}He cluster which has neutron halo. In the ordinary method, the ^{6}He cluster is often approximated by the $(0s)^4(0p_{3/2})^2$ configuration of HO wave function [67, 72].

(5) Laplace expansion method does not use the eigenvalue of norm kernel defined by Eq. (44), which represents the antisymmetrization effect between clusters. In general, the calculation of this quantity is not easy when the clusters are not described by the $SU(3)$ shell model wave functions. Therefore, several approximations have been suggested and applied [72, 76]. Laplace expansion method is free from such approximations.

The disadvantage of Laplace expansion method should be also commented. It is clear from Eq. (33), that the computational cost greatly increases when the mass of the system A is large

and the masses of clusters are equal ($C_1 = C_2$), because the number of possible combinations of $i_1, ..., i_A$ becomes huge. A typical example is the $^{16}\mathrm{O} + ^{16}\mathrm{O}$ cluster in $^{32}\mathrm{S}$. In this case, there are $(16!/(8!8!))^2 \simeq 1.6 \times 10^8$ combinations of $i_1, ..., i_A$. On the other hand, since $^{16}\mathrm{O}$ is a spherical and $SU(3)$ scalar cluster, the ordinary method can be straightforwardly applied and quickly calculated [82].

3 Numerical examples

In this section, we present the numerical results of the RWAs of the $^{16}\mathrm{O} + \alpha$ and $^{24}\mathrm{Mg} + \alpha$ clustering in $^{20}\mathrm{Ne}$ and $^{28}\mathrm{Si}$ which are composed of the unequal size clusters and deformed cluster. The wave functions of $^{20}\mathrm{Ne}$ and $^{28}\mathrm{Si}$ are calculated by the antisymmetrized molecular dynamics and the same with those obtained in our previous studies [41, 73, 83, 84]. The Hamiltonian is common to both nuclei and is given as,

$$\hat{H} = \sum_{i=1}^{A} \hat{t}_i - \hat{t}_{cm} + \sum_{i<j}^{A} \hat{v}_{NN} + \sum_{i<j}^{A} \hat{v}_{Coul}, \tag{47}$$

where $\hat{t}_i$ and $\hat{t}_{cm}$ denote the nucleon and the center-of-mass kinetic energies. $\hat{v}_{NN}$ and $\hat{v}_{Coul}$ denote the Gogny D1S effective nucleon-nucleon interaction [85] and the Coulomb interaction. The detailed set up of the calculations is explained below.

3.1 RWA of the $^{16}\mathrm{O} + \alpha$ clustering in $^{20}\mathrm{Ne}$

The $^{16}\mathrm{O} + \alpha$ clustering of $^{20}\mathrm{Ne}$ is very famous and experimentally identified well [16]. There are three rotational bands with $^{16}\mathrm{O} + \alpha$ cluster structure, which are built on the 0_1^+, 1_1^- (5.8 MeV) and 0_4^+ (8.7 MeV) states, respectively. Here we discuss the RWAs of the 0_1^+, 1_1^- and 0_4^+ states as an example of the unequal size clusters.

The AMD wave functions of $^{20}\mathrm{Ne}$ for GCM calculation are prepared by the energy variation with the constraint on the nuclear quadrupole deformation parameter β. The value of parameter β is constrained from 0.0 to 0.85 with an interval of 0.05. In addition to this, we also included Brink-Bloch type wave functions with the inter-cluster distance S_p ranging from 1.0 fm to 8.0 fm with an interval of 1.0 fm. Here, the $^{16}\mathrm{O}$ cluster is described by a single AMD wave function obtained by the energy variation, while α cluster is assumed to have $(0s)^4$ configuration. To analytically remove the center-of-mass motion from GCM wave function, both clusters are assumed to have the same spherical oscillator parameter $\nu = 0.16$ fm^{-2}. In short, we superposed 18 AMD wave functions and 8 Brink-Bloch type wave functions together, and solved the GCM. Thus-obtained level scheme is shown in Fig. 1 together

with the observed levels. The detailed discussions of these states are found in the Refs. [41, 73].

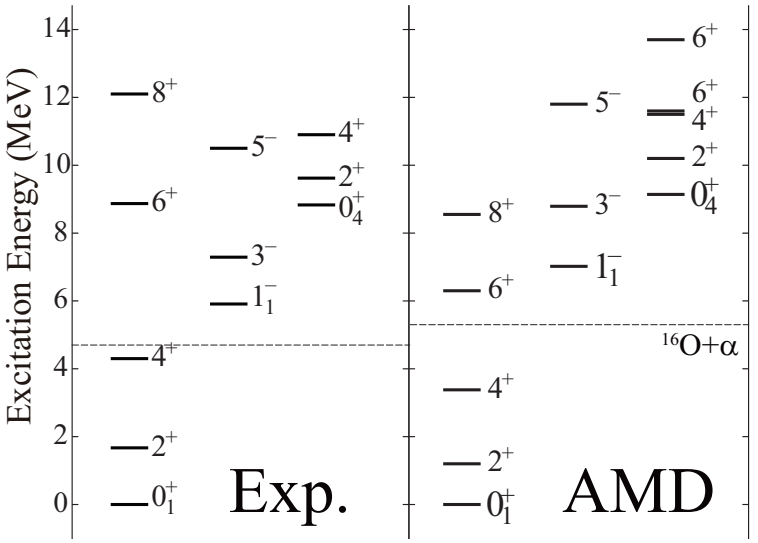

Fig. 1 The calculated and observed partial level scheme of ^{20}Ne corresponding to the $^{16}\mathrm{O}+\alpha$ cluster states. The dashed horizontal lines indicate experimental and theoretical $^{16}\mathrm{O}+\alpha$ cluster threshold energies.

We prepared two different sets of the cluster wave functions as the reference states ($\Phi^{j_1\pi_1}_{m_1C_1}$ and $\Phi^{j_2\pi_2}_{m_2C_2}$ in Eqs. (35) and (36)) to evaluate RWA. In the first set, ^{16}O and α clusters have the common oscillator lengths $\nu_{\mathrm{O}} = \nu_\alpha = 0.16$ fm^{-2}. Namely they are same with the above-mentioned Brink-Bloch type wave functions. In the second set, the oscillator lengths are different. For α cluster, we used $\nu_\alpha = 0.25$ fm^{-2}, while we used $\nu_{\mathrm{O}} = 0.157$ fm^{-2} for ^{16}O cluster which minimizes the intrinsic energy of ^{16}O. In the following, we denote the calculation with the first and second sets of the cluster wave functions by "common size calculation" and "unequal size calculation", respectively. In both cases the RWAs were calculated by the Laplace expansion method. The calculated RWAs for the 0^+_1, 0^+_2, and 1^-_1 states are shown in Fig. 2. And the α spectroscopic factor S_α and the dimensionless decay width θ^2 are listed in Table 1, which are defined as follows.

$$S_\alpha = \int_0^\infty da \left| a y^{J\pi}_{j_1\pi_1 j_2\pi_2 j_{12} l}(a) \right|^2, \tag{48}$$

$$\theta^2_\alpha = \frac{a}{3} \left| a y^{J\pi}_{j_1\pi_1 j_2\pi_2 j_{12} l}(a) \right|^2. \tag{49}$$

From larger amplitudes of the RWAs, S_α and θ_α, it is evident that the 0^+_4 and 1^-_1 states have more developed cluster structure than the ground state. When we compare the RWAs

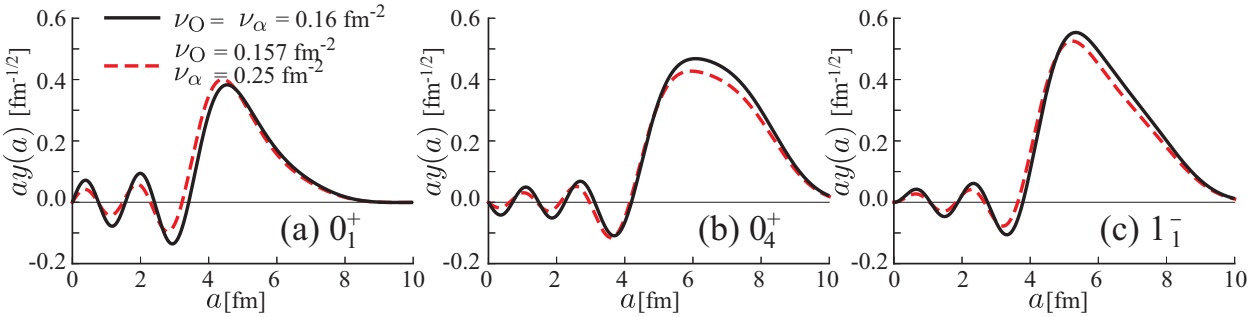

Fig. 2 The $^{16}\mathrm{O}+\alpha$ cluster RWAs of (a) the 0_1^+ state (b) the 0_4^+ state and (c) the 1_1^- state. The solid line show the RWAs obtained by using the reference states with common oscillator lengths $\nu_O = \nu_\alpha = 0.16$ fm^{-2}, while the dashed lines show those obtained by using the different oscillator parameters $\nu_O = 0.157$ fm^{-2} and $\nu_\alpha = 0.25$ fm^{-2}.

Table 1 The α spectroscopic factor S_α and the dimension decay width θ_α^2 calculated at the channel radii $a = 6$ and 7 fm.

	$\nu_O = \nu_\alpha = 0.16$ fm^{-2}			$\nu_O = 0.157$ fm^{-2}, $\nu_\alpha = 0.25$ fm^{-2}		
	S_α	θ_α^2 ($a = 6$ fm)	θ_α^2 ($a = 7$ fm)	S_α	θ_α^2 ($a = 6$ fm)	θ_α^2 ($a = 7$ fm)
0_1^+	0.24	0.06	0.01	0.26	0.05	0.01
0_4^+	0.62	0.44	0.43	0.53	0.37	0.35
1_1^-	0.71	0.49	0.28	0.63	0.41	0.22

obtained by the common size and unequal size calculations, we find the following differences, although they show similar behavior.

(1) The nodal points of RWA moves inward in the unequal size calculation.
(2) The amplitude of RWAs tend to be smaller in the unequal size calculation.

The first point is due to the weaker antisymmetrization effect. The unequal size calculation uses much smaller size of the α cluster than the common size calculation. Therefore, the α cluster is much less affected by the antisymmetrization effect. Since the oscillation of the RWAs in the internal region originates in the antisymmetrization effect, the nodal positions of RWA should move inward in the unequal calculation.

For the second point, there may be two explanations. In the inner region, the α clusters should be strongly distorted due to the strong effect of antisymmetrization and the mean-field potential. In such case, the size of α cluster should differ from that of free α particle and may be enlarged to gain the attraction from the mean-field potential. Therefore, the common size clusters may be favored in the inner region. In the outer region, the difference originates

in the defect of the present GCM calculation. To analytically remove the center-of-mass wave function, the wave packet sizes of AMD wave function are common to all nucleons. As a result, even at the large inter-cluster distance, the oscillator parameters for ^{16}O and α clusters are common in the GCM wave function, while they should be unequal to describe the correct asymptotics. It is evident that the common oscillator parameters of GCM wave function reduces the RWA in the outer region in the unequal size calculation. From these differences, compared to the common size calculation, the unequal size calculation tends to yield smaller values of S_α and θ_α by approximately 10 to 20% except for the ground state.

3.2 RWA of the ^{24}Mg + α clustering in ^{28}Si

A variety of cluster states such as the $^{24}\mathrm{Mg}+\alpha$, $^{20}\mathrm{Ne}+2\alpha$ and $^{16}\mathrm{O}+^{12}\mathrm{C}$ clustering are expected to exist in ^{28}Si. Many of them are related to the nuclear reactions in the astrophysical processes, and hence, have been intensively studied for many years [83, 84, 86–96], although their properties are not fully understood yet.

In our resent study [84], we have performed the AMD calculation to identify these cluster states. We made the energy variation with the constraint on the quadrupole deformation parameters β and γ [97] to generate the AMD wave functions for the GCM calculation. In addition to this, we also made the energy variation with the constraint on the inter-cluster distance [98] to generate various cluster configurations. These two kinds of basis wave functions are superposed and the GCM calculation was performed. As a result, we suggested various cluster bands; two groups of $^{24}\mathrm{Mg}+\alpha$ bands, the $^{20}\mathrm{Ne}+2\alpha$ and $^{16}\mathrm{O}+^{12}\mathrm{C}$ bands. Among them, we here discuss the RWAs of a group of $^{24}\mathrm{Mg}+\alpha$ bands, which was named "$^{24}\mathrm{Mg}+\alpha$ (T) bands" as an example of the deformed clusters.

Figure 3 (a) shows the $^{24}\mathrm{Mg}+\alpha$ (T) bands. Three rotational bands with pronounced $^{24}\mathrm{Mg}+\alpha$ clustering are built on the 1^-_1 and 0^+_6 states and on a group of 1^- states (1^-_8, 1^-_9 and 1^-_{10} states). Note that the $^{24}\mathrm{Mg}+\alpha$ configuration is strongly mixed with other cluster configurations such as $^{16}\mathrm{O}+^{12}\mathrm{C}$. As a result, it does not appear as a single state in the band built on the $1^-_{8,9,10}$ states. Therefore, in Fig. 3 (a), we show the averaged energy for the 3^-, 5^-, 7^- and 9^- states by the dotted lines. These three bands have large overlap with the basis wave function shown in Fig. 3 (c) in which the longest axis of the deformed ^{24}Mg cluster is perpendicular to the inter-cluster coordinate between ^{24}Mg and α clusters. The ground band is dominated by a mean-field configuration shown in Fig. 3 (b), but it also have non-negligible overlap with the cluster configuration shown in Fig. 3 (c). Therefore, the ground band was also assigned as a member of $^{24}\mathrm{Mg}+\alpha$ (T) bands. Because the ^{24}Mg cluster is considerably deformed, we expect the rotational excitation of ^{24}Mg is coupled to the angular momentum of the inter-cluster motion in RWAs. Experimentally, the corresponding cluster bands are

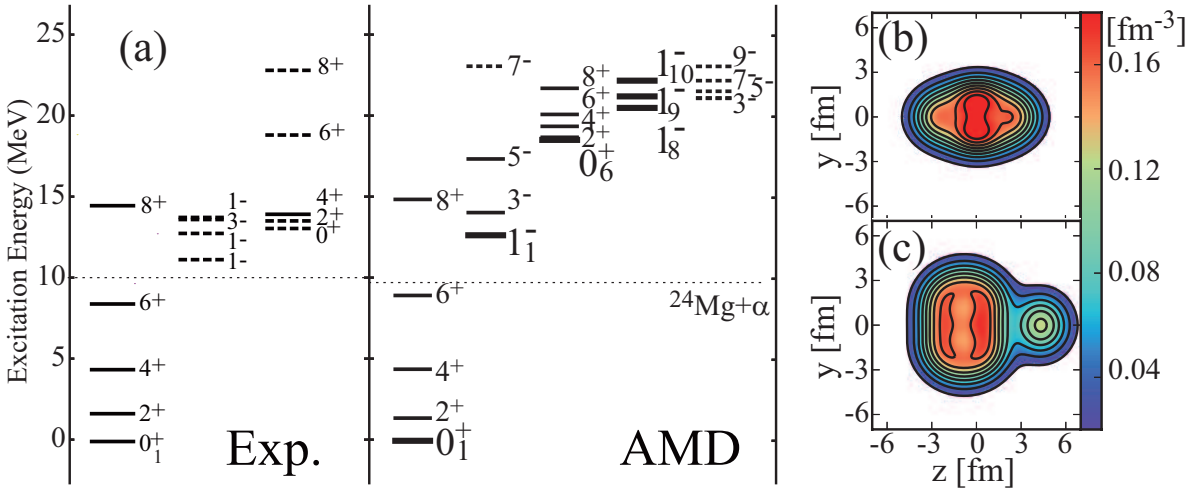

Fig. 3 (a) The calculated and observed partial level scheme of ^{28}Si corresponding to the $^{24}\mathrm{Mg}+\alpha$ cluster states. The dashed horizontal lines indicate experimental and theoretical $^{24}\mathrm{Mg}+\alpha$ threshold energies. (b) and (c) Intrinsic density distributions of the AMD wave functions which have the maximum overlap with the 0^+_1 and 0^+_6 states, respectively.

not clearly identified except for the ground band. In Fig. 3 we showed several candidates of the $^{24}\mathrm{Mg}+\alpha$ cluster states observed by the α transfer reaction on ^{24}Mg [89, 93].

To calculate the RWAs of the 0^+_1, 0^+_6, 1^-_1 and $1^-_{8,9,10}$ states, the cluster wave functions in the reference state are prepared as follows. The α cluster is assumed to have a $(0s)^4$ configuration and its spherical oscillator parameter is set to $\nu_\alpha = 0.25$ fm^{-2}. The AMD wave function for the ^{24}Mg cluster is calculated by the energy variation, and it is projected to the 0^+, 2^+ and 4^+ states. The oscillator parameter is determined to minimize the energy of the 0^+ state. Because of the triaxial deformation of the ^{24}Mg, the optimum oscillator parameter is anisotropic and have different values for the x, y and z directions as, $\boldsymbol{\nu}_{\mathrm{Mg}} = (0.12, 0.167, 0.169)$ fm^{-2}. Using these cluster wave functions, the RWA is calculated for various combinations of the angular momenta. Denoting the parity and the angular-momentum of ^{24}Mg by j^π and those of the inter-cluster motion by $l^{(-)^l}$, the RWAs of the 0^+ states are calculated for the combinations, $j^\pi \otimes l^{(-)^l} = 0^+ \otimes 0^+$, $2^+ \otimes 2^+$ and $4^+ \otimes 4^+$, and the RWAs of the 1^- states are calculated for $j^\pi \otimes l^{(-)^l} = 0^+ \otimes 1^-$, $2^+ \otimes 1^-$, $2^+ \otimes 3^-$, $4^+ \otimes 3^-$ and $4^+ \otimes 5^-$.

The results are presented in Fig. 4, Tabs. 2 and 3. Although the detailed discussions on RWAs and their relationship to the clustering in ^{28}Si will be made in our next work, we here briefly comment the characteristics of the calculated RWAs. The RWAs of the 0^+_1 and 1^- states show similar nature. These states are dominated by the mean-field configurations

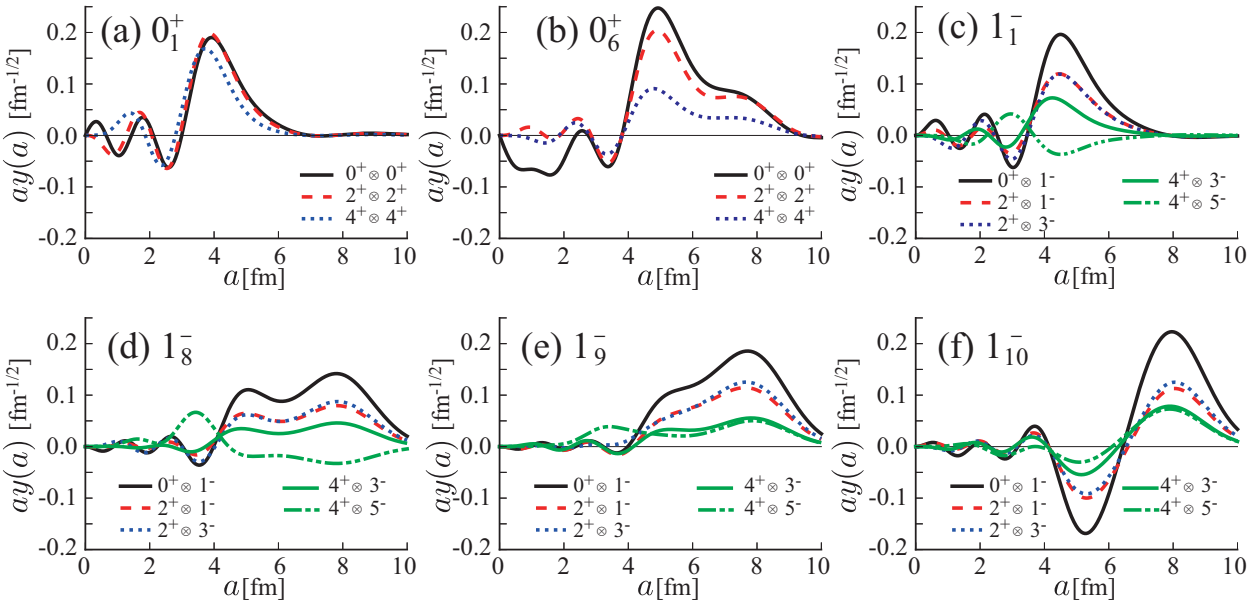

Fig. 4 The RWAs of the 0^+_1, 0^+_6, 1^-_8, 1^-_9 and 1^-_{10} states of ^{28}Si for ^{24}Mg+α cluster channels $j_2 \otimes l$ up to $j_2 = 4$ and $l = 5$.

Table 2 The calculated α spectroscopic factors S_α and the dimensionless decay widths θ^2_α of ^{24}Mg+α clustering in 0^+ states. The dimensionless decay widths are given in the unit of 10^{-2} and calculated with the channel radius $a = 5$ and 9 fm for the 0^+_1 and 0^+_6 states, respectively.

	S_α			θ^2_α		
$j^\pi \otimes l^{(-)^l}$	$0^+ \otimes 0^+$	$2^+ \otimes 2^+$	$4^+ \otimes 4^+$	$0^+ \otimes 0^+$	$2^+ \otimes 2^+$	$4^+ \otimes 4^+$
0^+_1	0.05	0.05	0.03	1.1	1.0	0.3
0^+_6	0.11	0.07	0.01	1.1	1.0	0.2

and under the strong influence of the spin-orbit interaction. Therefore, the clusters are considerably distorted and S_α is rather small. Nevertheless, we recognize non-negligible cluster formation probability around the surface region of the nucleus ($a \simeq 4$ fm), which indicates the duality of the shell and cluster as discussed in Ref. [84]. In terms of the $SU(3)$ shell model, the 0^+_1 and 1^-_1 states correspond to the $0\hbar\omega$ and $1\hbar\omega$ configurations, and hence, the nodal quantum number n of RWAs should be equal to $n = (N - l)/2$ where N is 8 and 9 for the 0^+_1 and 1^- states, respectively. We clearly see the calculated RWAs follow this relationship. Namely, for example, the $0^+ \otimes 0^+$ RWA has four nodes, while the $2^+ \otimes 2^+$ RWA has three.

Table 3 The calculated spectroscopic factors S_α and the dimensionless decay widths θ_α^2 of ^{24}Mg+α clustering in 1^- states. The dimensionless decay widths are given in the unit of 10^{-2} calculated with the channel radius $a = 6$ and 9 fm for the 1_1^- and $1_{8,9,10}^-$ states, respectively.

			S_α		
$j^\pi \otimes l^{(-)^l}$	$0^+ \otimes 1^-$	$2^+ \otimes 1^-$	$2^+ \otimes 3^-$	$4^+ \otimes 3^-$	$4^+ \otimes 5^-$
1_1^-	0.06	0.02	0.02	0.03	0.01
1_8^-	0.06	0.02	0.04	0.01	0.01
1_9^-	0.09	0.04	0.02	0.01	0.01
1_{10}^-	0.12	0.03	0.04	0.01	0.01
			θ_α^2		
$j^\pi \otimes l^{(-)^l}$	$0^+ \otimes 1^-$	$2^+ \otimes 1^-$	$2^+ \otimes 3^-$	$4^+ \otimes 3^-$	$4^+ \otimes 5^-$
1_1^-	0.8	0.3	0.3	0.2×10^{-1}	0.5×10^{-1}
1_8^-	1.9	0.6	0.8	0.2	0.2
1_9^-	3.0	1.1	1.3	0.3	0.3
1_{10}^-	5.0	1.5	0.2	0.6	0.5

Compared to the 0_1^+ and 1_1^- states, the 0_6^+ and $1_{8,9,10}^-$ states have developed cluster structure. It is confirmed from their larger S_α and RWAs stretched to the outward. Different from the 0_1^+ and 1_1^- states, their RWAs do not follow the relationship of $n = (N - l)/2$. This is due to the mixing with other cluster and non-cluster configurations, which disturbs the behavior of RWAs. Indeed, we see that RWAs, in particular those of the $1_{8,9,10}^-$ states, show irregular behavior in the inner and outer regions. This is consistent with the fact that the $^{24}\mathrm{Mg} + \alpha$ configuration is strongly mixed with non-cluster configurations and does not appear as a single state but appears as the $1_{8,9,10}^-$ states in this energy region. It is also noted that the RWAs in the $j^\pi \otimes l^{(-)^l} = 2^+ \otimes l^{(-)^l}$ and $4^+ \otimes l^{(-)^l}$ channels are as large as those of the $0^+ \otimes l^{(-)^l}$ channels, which reveals that the rotational excitation of ^{24}Mg is coupled to the inter-cluster motion, because of the large deformation of ^{24}Mg.

It must be emphasized that the RWAs shown in Fig. 4 are hardly obtained by the ordinary method because large computational cost is demanded. Thus, the Laplace expansion method realizes the accurate and detailed analysis of the clustering based on the RWAs, which is indispensable to discuss the clustering in heavier mass nuclei and unstable nuclei.

4 Summary

In summary, we presented a new method for the RWA calculation named Laplace expansion method. This method is based on the Laplace expansion and the analytical separation of the center-of-mass wave function, and applicable to the Brink-Bloch and AMD wave functions. The method enables the calculation of RWA for the different size clusters and deformed clusters without any approximations. Furthermore, it allows the use of the GCM wave function for the cluster wave functions, which enables to calculate the RWA of the non-conventional clusters such as ^{6}He. Despite of these advantages, the method does not require large computational cost except for the heavy mass clusters.

Using the Laplace expansion method, we calculated the RWAs of the $^{16}\mathrm{O} + \alpha$ clustering as an example of the unequal size clusters. It was found that the $^{16}\mathrm{O} + \alpha$ RWA calculated by using unequal size clusters tends to be smaller than the common size case, and the difference amounts to 10-20%. We also presented the RWAs of the $^{24}\mathrm{Mg} + \alpha$ clustering as an example of the deformed clusters. It was shown that the RWAs are considerably distorted, because of the mixing with the cluster and non-cluster configurations. The RWAs also showed that the rotational excitation of ^{24}Mg is coupled to the inter-cluster motion, because of the large deformation of ^{24}Mg. Thus, the Laplace expansion method enables the calculation of RWA for various cluster systems, and we expect it will be very helpful for the study of the clustering in heavier mass nuclei and unstale nuclei.

Acknowledgment

Insert the Acknowledgment text here.

References

[1] Kiyomi Ikeda, Noboru Takigawa, and Hisashi Horiuchi, Prog. Theor. Phys. Suppl., **E68**, 464–475 (1968).
[2] M. Seya, M. Kohno, and S. Nagata, Prog. Theor. Phys., **65**, 204–223 (1981).
[3] W. von Oertzen, Zeitschrift für Phys. A Hadron. Nucl., **354**, 37–43 (1996).
[4] Y. Kanada-En'yo, H. Horiuchi, and A. Doté, Phys. Rev. C, **60**, 064304 (1999).
[5] N. Itagaki and S. Okabe, Phys. Rev. C, **61**, 044306 (2000).
[6] P. Descouvemont, Nucl. Phys. A, **699**, 463–478 (2002).
[7] M. Freer, J. C. Angélique, L. Axelsson, B. Benoit, U. Bergmann, W. N. Catford, S. P. G. Chappell, N. M. Clarke, N. Curtis, A. D'Arrigo, E. de Goes Brennard, O. Dorvaux, B. R. Fulton, G. Giardina, C. Gregori, S. Grévy, F. Hanappe, G. Kelly, M. Labiche, C. Le Brun, S. Leenhardt, M. Lewitowicz, K. Markenroth, F. M. Marqués, M. Motta, J. T. Murgatroyd, T. Nilsson, A. Ninane, N. A. Orr, I. Piqueras, M. G. Saint Laurent, S. M. Singer, O. Sorlin, L. Stuttgé, and D. L. Watson, Phys. Rev. Lett., **82**, 1383–1386 (1999).
[8] M. Freer, J. C. Angélique, L. Axelsson, B. Benoit, U. Bergmann, W. N. Catford, S. P. G. Chappell, N. M. Clarke, N. Curtis, A. D'Arrigo, E. de Góes Brennard, O. Dorvaux, B. R. Fulton, G. Giardina, C. Gregori, S. Grévy, F. Hanappe, G. Kelly, M. Labiche, C. Le Brun, S. Leenhardt, M. Lewitowicz, K. Markenroth, F. M. Marqués, J. T. Murgatroyd, T. Nilsson, A. Ninane, N. A. Orr, I. Piqueras, M. G. Saint Laurent, S. M. Singer, O. Sorlin, L. Stuttgé, and D. L. Watson, Phys. Rev. C, **63**, 034301 (2001).
[9] N. Curtis, N. I. Ashwood, N. M. Clarke, M. Freer, C. J. Metelko, N. Soić, W. N. Catford, D. Mahboub, S. Pain, and D. C. Weisser, Phys. Rev. C, **70**, 014305 (2004).

[10] M. Milin, M. Zadro, S. Cherubini, T. Davinson, A. Di Pietro, P. Figuera, . Miljanić, A. Musumarra, A. Ninane, A.N. Ostrowski, M.G. Pellegriti, A.C. Shotter, N. Soić, and C. Spitaleri, Nucl. Phys. A, **753**, 263–287 (2005).
[11] H. G. Bohlen, T. Dorsch, Tz. Kokalova, W. von Oertzen, Ch. Schulz, and C. Wheldon, Phys. Rev. C, **75**, 054604 (2007).
[12] P Descouvemont and D Baye, Reports Prog. Phys., **73**, 036301 (2010).
[13] Fumiki Nemoto and Hiroharu Band\=o, Prog. Theor. Phys., **47**, 1210–1234 (1972).
[14] W. Sünkel and K. Wildermuth, Phys. Lett. B, **41**, 439–442 (1972).
[15] Takehiro Matsuse and Masayasu Kamimura, Prog. Theor. Phys., **49**, 1765–1767 (1973).
[16] Yoshikazu Fujiwara, Hisashi Horiuchi, Kiyomi Ikeda, Masayasu Kamimura, Kiyoshi Kat, Yasuyuki Suzuki, Eiji Uegaki, Kiyoshi Kato, Yasuyuki Suzuki, and Eiji Uegaki, Prog. Theor. Phys. Suppl., **68**, 29–192 (1980).
[17] P. Descouvemont and D. Baye, Phys. Rev. C, **36**, 54–59 (1987).
[18] U. Strohbusch, C. L. Fink, B. Zeidman, R. G. Markham, H. W. Fulbright, and R. N. Horoshko, Phys. Rev. C, **9**, 965–972 (1974).
[19] H. Friedrich and K. Langanke, Nucl. Phys. A, **252**, 47–61 (1975).
[20] R.R. Betts, H.T. Fortune, J.N. Bishop, M.N.I. Al-Jadir, and R. Middleton, Nucl. Phys. A, **292**, 281–287 (1977).
[21] H. T. Fortune, M. N. I. Al-Jadir, R. R. Betts, J. N. Bishop, and R. Middieton, Phys. Rev. C, **19**, 756–764 (1979).
[22] S. Ohkubo and K. Umehara, Prog. Theor. Phys., **80**, 598–600 (1988).
[23] T. Wada and H. Horiuchi, Phys. Rev. C, **38**, 2063–2077 (1988).
[24] T. Yamaya, S. Ohkubo, S. Okabe, and M. Fujiwara, Phys. Rev. C, **47**, 2389–2392 (1993).
[25] T. Yamaya, M. Saitoh, M. Fujiwara, T. Itahashi, K. Katori, T. Suehiro, S. Kato, S. Hatori, and S. Ohkubo, Nucl. Phys. A, **573**, 154–172 (1994).
[26] F. Michel, S. Ohkubo, and G. Reidemeister, Prog. Theor. Phys. Suppl., **132**, 7–72 (1998).
[27] T. Yamaya, K. Katori, M. Fujiwara, S. Kato, and S. Ohkubo, Prog. Theor. Phys. Suppl., **132**, 73–102 (1998).
[28] Masaaki Kimura and Hisashi Horiuchi, Nucl. Phys. A, **767**, 58–80 (2006).
[29] A. Tohsaki, H. Horiuchi, P. Schuck, and G. Röpke, Phys. Rev. Lett., **87**, 192501 (2001).
[30] T. Kawabata, H. Akimune, H. Fujita, Y. Fujita, M. Fujiwara, K. Hara, K. Hatanaka, M. Itoh, Y. Kanada-En'yo, S. Kishi, K. Nakanishi, H. Sakaguchi, Y. Shimbara, A. Tamii, S. Terashima, M. Uchida, T. Wakasa, Y. Yasuda, H.P. Yoshida, and M. Yosoi, 2α+t cluster structure in 11B (2007).
[31] Yoshiko Kanada-En'yo, Phys. Rev. C, **75**(2), 024302 (feb 2007).
[32] T. Wakasa, E. Ihara, K. Fujita, Y. Funaki, K. Hatanaka, H. Horiuchi, M. Itoh, J. Kamiya, G. Röpke, H. Sakaguchi, N. Sakamoto, Y. Sakemi, P. Schuck, Y. Shimizu, M. Takashina, S. Terashima, A. Tohsaki, M. Uchida, H.P. Yoshida, and M. Yosoi, Phys. Lett. B, **653**, 173–177 (2007).
[33] T. KAWABATA, Y. SASAMOTO, Y. MAEDA, S. SAKAGUCHI, Y. SHIMIZU, K. SUDA, T. UESAKA, M. FUJIWARA, H. HASHIMOTO, K. HATANAKA, K. KAWASE, H. MATSUBARA, K. NAKANISHI, Y. TAMESHIGE, A. TAMII, K. ITOH, M. ITOH, H. P. YOSHIDA, Y. KANADA-EN'YO, and M. UCHIDA, Int. J. Mod. Phys. E, **17**, 2071–2075 (2008).
[34] Y. Funaki, T. Yamada, H. Horiuchi, G. Röpke, P. Schuck, and A. Tohsaki, Phys. Rev. Lett., **101**, 082502 (2008).
[35] M. Itoh, H. Akimune, M. Fujiwara, U. Garg, N. Hashimoto, T. Kawabata, K. Kawase, S. Kishi, T. Murakami, K. Nakanishi, Y. Nakatsugawa, B. K. Nayak, S. Okumura, H. Sakaguchi, H. Takeda, S. Terashima, M. Uchida, Y. Yasuda, M. Yosoi, and J. Zenihiro, Phys. Rev. C, **84**, 054308 (2011).
[36] T. Yamada, Y. Funaki, H. Horiuchi, K. Ikeda, and A. Tohsaki, Prog. Theor. Phys., **120**(6), 1139–1167 (dec 2008).
[37] T Kawabata, T Adachi, M Fujiwara, K Hatanaka, Y Ishiguro, M Itoh, Y Maeda, H Matsubara, H Miyasako, Y Nozawa, T Saito, S Sakaguchi, Y Sasamoto, Y Shimizu, T Takahashi, A Tamii, S Terashima, H Tokieda, N Tomida, T Uesaka, M Uchida, Y Yasuda, N Yokota, H P Yoshida, and J Zenihiro, J. Phys. Conf. Ser., **436**, 012009 (2013).
[38] M. Itoh, S. Kishi, H. Sakaguchi, H. Akimune, M. Fujiwara, U. Garg, K. Hara, H. Hashimoto, J. Hoffman, T. Kawabata, K. Kawase, T. Murakami, K. Nakanishi, B. K. Nayak, S. Terashima, M. Uchida, Y. Yasuda, and M. Yosoi, Phys. Rev. C, **88**, 064313 (2013).
[39] Y. Chiba and M. Kimura, Phys. Rev. C, **91**(6), 061302 (jun 2015).
[40] Yoshiko Kanada-En'yo, Phys. Rev. C, **93**(5), 054307 (may 2016).
[41] Y. Chiba, M. Kimura, and Y. Taniguchi, Phys. Rev. C, **93**, 034319 (2016).
[42] W. Scholz, P. Neogy, K. Bethge, and R. Middleton, Phys. Rev. C, **6**, 893–900 (1972).
[43] P. Descouvemont and D. Baye, Phys. Rev. C, **31**, 2274–2284 (1985).
[44] P. Descouvemont, Phys. Rev. C, **38**, 2397–2407 (1988).
[45] G. V. Rogachev, V. Z. Goldberg, T. Lönnroth, W. H. Trzaska, S. A. Fayans, K.-M. Källman, J. J. Kolata,

M. Mutterer, M. V. Rozhkov, and B. B. Skorodumov, Phys. Rev. C, **64**, 051302 (2001).
[46] N. Curtis, D. D. Caussyn, C. Chandler, M. W. Cooper, N. R. Fletcher, R. W. Laird, and J. Pavan, Phys. Rev. C, **66**, 024315 (2002).
[47] V. Z. Goldberg, G. V. Rogachev, W. H. Trzaska, J. J. Kolata, A. Andreyev, C. Angulo, M. J. G. Borge, S. Cherubini, G. Chubarian, G. Crowley, P. Van Duppen, M. Gorska, M. Gulino, M. Huyse, P. Jesinger, K.-M. Källman, M. Lattuada, T. Lönnroth, M. Mutterer, R. Raabe, S. Romano, M. V. Rozhkov, B. B. Skorodumov, C. Spitaleri, O. Tengblad, and A. Tumino, Phys. Rev. C, **69**, 024602 (2004).
[48] S. Yildiz, M. Freer, N. Soić, S. Ahmed, N. I. Ashwood, N. M. Clarke, N. Curtis, B. R. Fulton, C. J. Metelko, B. Novatski, N. A. Orr, R. Pitkin, S. Sakuta, and V. A. Ziman, Phys. Rev. C, **73**, 034601 (2006).
[49] Masaaki Kimura, Phys. Rev. C, **75**, 034312 (2007).
[50] N. Furutachi, M. Kimura, A. Dote, Y. Kanada-En'yo, and S. Oryu, Prog. Theor. Phys., **119**, 403–420 (2008).
[51] Changbo Fu, V. Z. Goldberg, G. V. Rogachev, G. Tabacaru, G. G. Chubarian, B. Skorodumov, M. McCleskey, Y. Zhai, T. Al-Abdullah, L. Trache, and R. E. Tribble, Phys. Rev. C, **77**, 064314 (2008).
[52] E. D. Johnson, G. V. Rogachev, V. Z. Goldberg, S. Brown, D. Robson, A. M. Crisp, P. D. Cottle, C. Fu, J. Giles, B. W. Green, K. W. Kemper, K. Lee, B. T. Roeder, and R. E. Tribble, Eur. Phys. J. A, **42**, 135 (2009).
[53] W. von Oertzen, T. Dorsch, H. G. Bohlen, R. Krücken, T. Faestermann, R. Hertenberger, Tz. Kokalova, M. Mahgoub, M. Milin, C. Wheldon, and H. F. Wirth, Eur. Phys. J. A, **43**, 17 (2010).
[54] N. Soić, M. Freer, L. Donadille, N. M. Clarke, P. J. Leask, W. N. Catford, K. L. Jones, D. Mahboub, B. R. Fulton, B. J. Greenhalgh, D. L. Watson, and D. C. Weisser, Phys. Rev. C, **68**, 014321 (2003).
[55] W. von Oertzen, H. G. Bohlen, M. Milin, Tz Kokalova, S. Thummerer, A. Tumino, R. Kalpakchieva, T. N. Massey, Y. Eisermann, G. Graw, T. Faestermann, R. Hertenberger, and H.-F. Wirth, Eur. Phys. J. A, **21**, 193–215 (2004).
[56] D. L. Price, M. Freer, N. I. Ashwood, N. M. Clarke, N. Curtis, L. Giot, V. Lima, P. Mc Ewan, B. Novatski, N. A. Orr, S. Sakuta, J. A. Scarpaci, D. Stepanov, and V. Ziman, Phys. Rev. C, **75**, 014305 (2007).
[57] P. J. Haigh, N. I. Ashwood, T. Bloxham, N. Curtis, M. Freer, P. McEwan, D. Price, V. Ziman, H. G. Bohlen, Tz. Kokalova, Ch. Schulz, R. Torabi, W. von Oertzen, C. Wheldon, W. Catford, C. Harlin, R. Kalpakchieva, and T. N. Massey, Phys. Rev. C, **78**, 014319 (2008).
[58] Tadahiro Suhara and Yoshiko Kanada-En'yo, Phys. Rev. C, **82**, 044301 (2010).
[59] M. Freer, J. D. Malcolm, N. L. Achouri, N. I. Ashwood, D. W. Bardayan, S. M. Brown, W. N. Catford, K. A. Chipps, J. Cizewski, N. Curtis, K. L. Jones, T. Munoz-Britton, S. D. Pain, N. Soić, C. Wheldon, G. L. Wilson, and V. A. Ziman, Phys. Rev. C, **90**, 054324 (2014).
[60] T. Baba, Y. Chiba, and M. Kimura, Phys. Rev. C, **90**, 064319 (2014).
[61] Z. Y. Tian, Y. L. Ye, Z. H. Li, C. J. Lin, Q. T. Li, Y. C. Ge, J. L. Lou, W. Jiang, J. Li, Z. H. Yang, J. Feng, P. J. Li, J. Chen, Q. Liu, H. L. Zang, B. Yang, Y. Zhang, Z. Q. Chen, Y. Liu, X. H. Sun, J. Ma, H. M. Jia, X. X. Xu, L. Yang, N. R. Ma, and L. J. Sun, Chinese Phys. C, **40**, 111001 (2016).
[62] D. Dell'Aquila, I. Lombardo, L. Acosta, R. Andolina, L. Auditore, G. Cardella, M. B. Chatterjiee, E. De Filippo, L. Francalanza, B. Gnoffo, G. Lanzalone, A. Pagano, E. V. Pagano, M. Papa, S. Pirrone, G. Politi, F. Porto, L. Quattrocchi, F. Rizzo, E. Rosato, P. Russotto, A. Trifirò, M. Trimarchi, G. Verde, and M. Vigilante, Phys. Rev. C, **93**, 024611 (2016).
[63] A. Fritsch, S. Beceiro-Novo, D. Suzuki, W. Mittig, J. J. Kolata, T. Ahn, D. Bazin, F. D. Becchetti, B. Bucher, Z. Chajecki, X. Fang, M. Febbraro, A. M. Howard, Y. Kanada-En'yo, W. G. Lynch, A. J. Mitchell, M. Ojaruega, A. M. Rogers, A. Shore, T. Suhara, X. D. Tang, R. Torres-Isea, and H. Wang, Phys. Rev. C, **93**, 014321 (2016).
[64] T. Baba and M. Kimura, Phys. Rev. C, **94**, 044303 (2016).
[65] H. Yamaguchi, D. Kahl, S. Hayakawa, Y. Sakaguchi, K. Abe, T. Nakao, T. Suhara, N. Iwasa, A. Kim, D.H. Kim, S.M. Cha, M.S. Kwag, J.H. Lee, E.J. Lee, K.Y. Chae, Y. Wakabayashi, N. Imai, N. Kitamura, P. Lee, J.Y. Moon, K.B. Lee, C. Akers, H.S. Jung, N.N. Duy, L.H. Khiem, and C.S. Lee, Phys. Lett. B, **766**, 11–16 (2017).
[66] J. Li, Y. L. Ye, Z. H. Li, C. J. Lin, Q. T. Li, Y. C. Ge, J. L. Lou, Z. Y. Tian, W. Jiang, Z. H. Yang, J. Feng, P. J. Li, J. Chen, Q. Liu, H. L. Zang, B. Yang, Y. Zhang, Z. Q. Chen, Y. Liu, X. H. Sun, J. Ma, H. M. Jia, X. X. Xu, L. Yang, N. R. Ma, and L. J. Sun, Phys. Rev. C, **95**, 021303 (2017).
[67] Tomoyuki Baba and Masaaki Kimura (2017), 1702.04874.
[68] V. V. Balashov, V. G. Neudachin, Yu. F. Smirnov, and N. P. Yudin, Jounal Exp. Theor. Phys., **37**, 1385 (1959).
[69] T. Honda, H. Horie, Y. Kudo, and H. UI, Nucl. Phys., **62**, 561–574 (1965).
[70] Hisashi Horiuchi, Prog. Theor. Phys., **47**, 1058–1060 (1972).
[71] Hisashi Horiuchi, Prog. Theor. Phys. Suppl., **62**, 90–190 (1977).
[72] Y. Kanada-En'yo and H. Horiuchi, Phys. Rev. C, **68**, 014319 (2003).
[73] Masaaki Kimura, Phys. Rev. C, **69**(4), 044319 (2004).

[74] J. P. Elliott, Proc. R. Soc. London A Math. Phys. Eng. Sci., **245**(1240) (1958).
[75] J. P. Elliott, Proc. R. Soc. London A Math. Phys. Eng. Sci., **245**(1243) (1958).
[76] Y. Kanada-En'yo, T. Suhara, and Y. Taniguchi, Prog. Theor. Exp. Phys., **2014**, 73D02–0 (2014).
[77] Yoshiko Kanada-En'yo, Masaaki Kimura, and Hisashi Horiuchi, Comptes Rendus Phys., **4**, 497–520 (2003).
[78] Y. Kanada-En'yo, M. Kimura, and A. Ono, Prog. Theor. Exp. Phys., **2012**(1), 1A202–0 (jan 2012).
[79] M. Kimura, T. Suhara, and Y. Kanada-En'yo, Eur. Phys. J. A, **52**, 373 (2016).
[80] D. M. Brink, *Proc. Int. School of Physics Enrico Fermi, Course 36, Varenna,*, (Academic Press, New York, 1966).
[81] A. Tohsaki-Suzuki, Prog. Theor. Phys., **59**, 1261–1275 (1978).
[82] Masaaki Kimura and Hisashi Horiuchi, Phys. Rev. C, **69**, 051304 (2004).
[83] Yasutaka Taniguchi, Yoshiko Kanada-En'yo, and Masaaki Kimura, Phys. Rev. C, **80**(4), 044316 (oct 2009).
[84] Y. Chiba, Y. Taniguchi, and M. Kimura (2016), 1610.04000.
[85] J.F. Berger, M. Girod, and D. Gogny, Comput. Phys. Commun., **63**(1), 365–374 (1991).
[86] R. Stokstad, D. Shapira, L. Chua, P. Parker, M. W. Sachs, R. Wieland, and D. A. Bromley, Phys. Rev. Lett., **28**, 1523–1525 (1972).
[87] D. Baye, Nucl. Phys. A, **272**, 445–465 (1976).
[88] J.W. Maas, E. Somorjai, H.D. Graber, C.A. Van Den Wijngaart, C. Van Der Leun, and P.M. Endt, Nucl. Phys. A, **301**, 213–236 (1978).
[89] J. Cseh, E. Koltay, Z. Máté, E. Somorjai, and L. Zolnai, Nucl. Phys. A, **385**, 43–56 (1982).
[90] T. Tanabe, K. Haga, M. Yasue, K. Sato, K. Ogino, Y. Kadota, M. Tochi, K. Makino, T. Kitahara, and T. Shiba, Nucl. Phys. A, **399**, 241–258 (1983).
[91] K. Kato, S. Okabe, and Y. Abe, Prog. Theor. Phys., **74**, 1053–1076 (1985).
[92] S. Kubono, K. Morita, M.H. Tanaka, A. Sakaguchi, M. Sugitani, and S. Kato, Nucl. Phys. A, **457**, 461–476 (1986).
[93] K. P. Artemov, M. S. Golovkov, V. Z. Goldberg, V. I. Dukhanov, I. B. Mazurov, V. V. Pankratov, V. V. Paramonov, V. P. Rudakov, I. N. Serikov, V. A. Solovev, and V. A. Timofeev, Sov. J. Nucl. Phys., **51**, 777 (1990).
[94] N. I. Ashwood, J. T. Murgatroyd, N. M. Clarke, M. Freer, B. R. Fulton, A. St. J. Murphy, S. P. G. Chappell, R. L. Cowin, G. K. Dillon, D. L. Watson, W. N. Catford, N. Curtis, M. Shawcross, and V. Pucknell, Phys. Rev. C, **63**, 034315 (2001).
[95] M. Shawcross, N. Curtis, W. N. Catford, N. M. Clarke, B. R. Fulton, S. J. Hall, J. T. Murgatroyd, S. P. G. Chappell, R. L. Cowin, G. Dillon, and D. L. Watson, Phys. Rev. C, **63**, 034311 (2001).
[96] A. Goasduff, S. Courtin, F. Haas, D. Lebhertz, D. G. Jenkins, J. Fallis, C. Ruiz, D. A. Hutcheon, P.-A. Amandruz, C. Davis, U. Hager, D. Ottewell, and G. Ruprecht, Phys. Rev. C, **89**, 014305 (2014).
[97] M. Kimura, R. Yoshida, and M. Isaka, Prog. Theor. Phys., **127**(2), 287–301 (2012).
[98] Y. Taniguchi, M. Kimura, and H. Horiuchi, Prog. Theor. Phys., **112**, 475–487 (2004).

A Calculataion of the overlaps needed in the Laplace expansion method

Here, we explain the calculation of the overlaps defined by Eqs. (34), (35) and (36). For arbitrary matrix Γ, Eq. (34) is calculated by the numerical integration,

$$\chi_{lm_l}(a; i_1, ..., i_A) = \left(\frac{|2\Gamma|}{\pi^3}\right)^{1/4} \int d\hat{r} Y^*_{lm_l}(\hat{r}) \exp\left\{-(\boldsymbol{r}-\boldsymbol{z})^T\Gamma(\boldsymbol{r}-\boldsymbol{z})\right\}. \tag{A1}$$

However, when $\chi(\boldsymbol{r}; i_1, ..., i_A)$ is a spherical Gaussian, *i.e.*, when the matrix Γ is proportional to the identity matrix I as $\Gamma = \gamma I$, Eq. (A1) has a simple analytical form,

$$\chi_{lm_l}(r; i_1, ..., i_A) = 4\pi i_l(2\gamma r z) e^{-\gamma(r^2+z^2)} \frac{z^l Y^*_{lm_l}(\hat{z})}{z^l}, \tag{A2}$$

where $i_l(2\gamma r z)$ denotes the regular modified spherical Bessel function. The complex variable z is defined as $z = \sqrt{\boldsymbol{z}\cdot\boldsymbol{z}}$ and $z^l Y^*_{lm_l}(\hat{z})$ should be calculated in its Cartesian representation.

The overlap $N^{j_1\pi_1}_{m_1}(i_1,...,i_{C_1})$ defined by Eq. (35) is calculated as follows. For simplicity, we first assume that the wave function $\Phi^{j_1\pi_1}_{m_1C_1}$ in the reference state is also represented by a single projected AMD wave function,

$$\Phi^{AMD}_{C_1} = \Phi^{cm}_{C_1}\Phi^{int}_{C_1} = \frac{1}{\sqrt{C_1!}}\begin{vmatrix} \langle \boldsymbol{r}_1|\phi_{i_1}\rangle & \dots & \langle \boldsymbol{r}_1|\phi_{i_{C_1}}\rangle \\ \vdots & \ddots & \vdots \\ \langle \boldsymbol{r}_{C_1}|\phi_{i_1}\rangle & \dots & \langle \boldsymbol{r}_{C_1}|\phi_{i_{C_1}}\rangle \end{vmatrix}, \tag{A3}$$

$$\Phi^{cm}_{C_1} = \left(\frac{|2C_1 m|}{\pi^3}\right)^{1/4}\exp\left\{-C_1\boldsymbol{r}^T m\boldsymbol{r}\right\}, \tag{A4}$$

$$\Phi^{j_1\pi_1}_{m_1C_1} = \frac{1}{\sqrt{n^{j_1\pi_1}_{k_1}}}\hat{P}^{j_1}_{m_1k_1}\hat{P}^{\pi_1}\Phi^{int}_{C_1}, \quad n^{j_1\pi_1}_{k_1} = \langle\Phi^{int}_{C_1}|\hat{P}^{j_1\pi_1}_{k_1k_1}|\Phi^{int}_{C_1}\rangle\,. \tag{A5}$$

Then, the overlap is given as

$$N^{j_1\pi_1}_{m_1}(i_1,...,i_{C_1}) = \frac{2j_1+1}{8\pi^2\sqrt{n^{j_1\pi_1}_{k_1}}}\int d\Omega D^{j_1*}_{k_1m_1}(\Omega)\,\langle\Phi^{int}_{C_1}|\hat{P}^{\pi_1}\hat{R}(\Omega)|\Psi^{int}_{C_1}(i_1,...,i_{C_1})\rangle\,, \tag{A6}$$

where the integration over Euler angles are numerically calculated. To calculate the integrand in Eq. (A6), we introduce an AMD wave function $\widetilde{\Psi}^{AMD}_{C_1}$

$$\widetilde{\Psi}^{AMD}_{C_1}(i_1,...,i_{C_1}) = \widetilde{\Psi}^{cm}_{C_1}\Psi^{int}_{C_1}(i_1,...,i_{C_1}) = \frac{1}{\sqrt{C_1!}}\begin{vmatrix} \langle \boldsymbol{r}_1|\widetilde{\psi}_{i_1}\rangle & \dots & \langle \boldsymbol{r}_1|\widetilde{\psi}_{i_{C_1}}\rangle \\ \vdots & \ddots & \vdots \\ \langle \boldsymbol{r}_{C_1}|\widetilde{\psi}_{i_1}\rangle & \dots & \langle \boldsymbol{r}_{C_1}|\widetilde{\psi}_{i_{C_1}}\rangle \end{vmatrix}, \tag{A7}$$

$$\langle\boldsymbol{r}|\widetilde{\psi}_i\rangle = \left(\frac{|2M|}{\pi^3}\right)^{1/4}\exp\left\{-(\boldsymbol{r}-\boldsymbol{Z}'_i)^T M(\boldsymbol{r}-\boldsymbol{Z}'_i)\right\}(\alpha_i\chi_\uparrow+\beta_i\chi_\downarrow)\eta_i, \tag{A8}$$

$$\widetilde{\Psi}^{cm}_{C_1} = \left(\frac{|2C_1M|}{\pi^3}\right)^{1/4}\exp\left\{-C_1\boldsymbol{R}^T_{C_1}M\boldsymbol{R}_{C_1}\right\}, \tag{A9}$$

$$\boldsymbol{Z}'_i = \boldsymbol{Z}_i - \frac{1}{C_1}\sum_{j\in i_1,...,i_{C_1}}\boldsymbol{Z}_j, \quad i\in\{i_1,...,i_{C_1}\}, \tag{A10}$$

where that the the Gaussian centroids are shifted from the original ones so that the center-of-mass wave function is located at the origin of the coordinate system. Note that this shift does not change the internal wave function. Therefore, the internal wave function of $\widetilde{\Psi}^{AMD}_{C_1}$ is same with the ket state of the integrant in Eq. (A6). Using Eqs. (A3) and (A7), the overlap of AMD wave functions is calculated as,

$$\langle\Phi^{AMD}_{C_1}|\hat{P}^{\pi}\hat{R}(\Omega)|\Psi^{AMD}_{C_1}\rangle = \langle\Phi^{int}_{C_1}|\hat{P}^{\pi}\hat{R}(\Omega)|\Psi^{int}_{C_1}\rangle\,\langle\Phi^{cm}_{C_1}|\hat{P}^{\pi}\hat{R}(\Omega)|\Psi^{cm}_{C_1}\rangle\,. \tag{A11}$$

Here the calculation of the left hand side of Eq. (A11) is straightforward, and the overlap of the center-of-mass wave functions is analytically calculated as,

$$\langle \Phi^{cm}_{C_1} | \hat{P}^{\pi} \hat{R}(\Omega) | \Psi^{cm}_{C_1} \rangle = \left(\frac{|2m||2M|}{|M' + m|^2} \right)^{1/4}, \tag{A12}$$

$$M' = R^T(\Omega) M R(\Omega), \tag{A13}$$

where $R(\Omega)$ is a 3×3 rotation matrix which satisfies $\hat{R}(\Omega)\boldsymbol{R} = R(\Omega)\boldsymbol{R}$. Therefore, the integrand is proportional to the overlap of AMD wave functions.

$$\langle \Phi^{int}_{C_1} | \hat{P}^{\pi} \hat{R}(\Omega) | \Psi^{int}_{C_1} \rangle = \left(\frac{|M' + m|^2}{|2m||2M|} \right)^{1/4} \langle \Phi^{AMD}_{C_1} | \hat{P}^{\pi} \hat{R}(\Omega) | \Psi^{AMD}_{C_1} \rangle \,. \tag{A14}$$

It is clear that when $\Phi^{j_1\pi_1}_{C_1}$ and/or $\Psi^{j_1\pi_1}_{C_1}$ are not single AMD wave function, but GCM wave function, the integrand is a superposition of Eq. (A14).

B An ordinary method for RWA calculation

For the sake of the self-containdness, we explain an ordinary method for RWA calculation [70–73] which is often used in the cluster models and AMD, and derive Eqs. (43), (44), (45) and (46). We start from a set of the Brink-Bloch type wave functions given in Eq. (40),

$$\Phi^{BB}_{j_1\pi_1 m_1 j_2\pi_2 m_2}(S_p) = n_0 \mathcal{A} \left\{ \hat{P}^{j_1}_{m_1 k_1} \hat{P}^{\pi_1} \Phi_{C_1}\left(-\frac{C_2}{A}\boldsymbol{S}_p \right) \hat{P}^{j_2}_{m_2 k_2} \hat{P}^{\pi_2} \Phi_{C_2}\left(\frac{C_1}{A}\boldsymbol{S}_p \right) \right\}, \tag{B1}$$

$$n_0 = \sqrt{\frac{C_1! C_2!}{A!}}, \quad \boldsymbol{S}_p = (0, 0, S_p), \tag{B2}$$

where $\Phi_{C_1}\,(-C_2/A\boldsymbol{S}_p)$ and $\Phi_{C_2}\,(C_1/A\boldsymbol{S}_p)$ are the wave functions for clusters with masses C_1 and C_2, and placed with the inter-cluster distance S_p. They are respectively projected to j^{π_1} and j^{π_2}. By assuming that Φ_{C_1} and Φ_{C_2} are the $SU(3)$ shell model wave functions without any particle-hole excitations and have the common oscillator parameter $\hbar\omega = 2\hbar^2\nu/m$, their internal and center-of-mass wave functions can be analytically separated,

$$\Phi_{C_1}\left(-\frac{C_2}{A}\boldsymbol{S}_p \right) = \Phi^{int}_{C_1} \Phi^{cm}_{C_1}, \quad \Phi^{cm}_{C_1} = \left(\frac{2C_1\nu}{\pi} \right)^{3/4} \exp\left\{ -C_1\nu(\boldsymbol{R}_{C_1} + \frac{C_2}{A}\boldsymbol{S}_p)^2 \right\}, \tag{B3}$$

$$\Phi_{C_2}\left(\frac{C_1}{A}\boldsymbol{S}_p \right) = \Phi^{int}_{C_2} \Phi^{cm}_{C_2}, \quad \Phi^{cm}_{C_2} = \left(\frac{2C_2\nu}{\pi} \right)^{3/4} \exp\left\{ -C_2\nu(\boldsymbol{R}_{C_2} - \frac{C_1}{A}\boldsymbol{S}_p)^2 \right\}, \tag{B4}$$

where $\boldsymbol{R}_{C_1}$ and $\boldsymbol{R}_{C_2}$ are the center-of-mass coordinates of clusters defined by Eq. (22). In a similar way to Eq. (24), we rewrite the product of the center-of-mass wave functions as

follows,

$$\Phi^{cm}_{C_1}\Phi^{cm}_{C_2} = \Phi^{cm}_{A}\chi(\boldsymbol{r}), \tag{B5}$$

$$\Phi^{cm}_{A} = \left(\frac{2A\nu}{\pi}\right)^{3/4}\exp\left\{-A\nu R^2\right\}, \tag{B6}$$

$$\chi(\boldsymbol{r}) = \left(\frac{2\gamma}{\pi}\right)^{3/4}\exp\left\{-\gamma(\boldsymbol{r}-\boldsymbol{S}_p)^2\right\}, \quad \gamma = \frac{C_1C_2}{A}\nu. \tag{B7}$$

Here $\boldsymbol{R}$ and $\boldsymbol{r}$ are the center-of-mass coordinate of A-body system and the inter-cluster coordinate defined by Eqs. (5) and (26), respectively. Note that the oscillator parameters of clusters should be the same. Otherwise the decomposition to the center-of-mass and relative coordinates is not straightforward. Since the relative wave function Eq. (B7) is the coherent state of HO except for a phase factor, it is represented by a superposition of the HO wave functions [71],

$$\chi(\boldsymbol{r}) = \sum_{Nl} a_{Nl}(S_p)R_{Nl}(r)Y_{l0}(\hat{r}), \tag{B8}$$

$$a_{Nl}(S_p) = (-)^{(N-l)/2}\sqrt{\frac{(2l+1)N!}{(N-l)!!(N+l+1)!!}}\frac{(\gamma S_p^2)^{N/2}}{\sqrt{N!}}e^{-\gamma S_p^2/2}, \tag{B9}$$

where $R_{Nl}(r)$ is the radial wave function of HO and N denotes the principal quantum number. With these equations, Brink-Bloch type wave function is rewritten as follows,

$$\Phi^{BB}_{j_1\pi_1 m_1 j_2\pi_2 m_2}(S_p) = \Phi^{cm}_{A}\sum_{Nl} a_{Nl}(S_p)n_0\mathcal{A}\left\{\, R_{Nl}(r)Y_{l0}(\hat{r})\Phi^{j_1}_{C_1m_1}\Phi^{j_2}_{C_2m_2}\,\right\}. \tag{B10}$$

Then, by using the property of the angular momentum projector $P^J_{MK}\,|JK\rangle = |JM\rangle$ and the coupling of angular momenta, we introduce the wave function,

$$\begin{aligned}\Phi^{J\pi}_{j_1\pi_1 j_2\pi_2 j_{12} l}(S_p) &= \frac{2l+1}{2J+1}\sum_{m_{12}m_1m_2} C^{Jm_{12}}_{l0m_{12}}\hat{P}^J_{Mm_{12}}C^{j_{12}m_{12}}_{j_1m_1j_2m_2}\Phi^{BB}_{j_1\pi_1m_1j_2\pi_2m_2}(S_p)\\ &= \sum_N a_{Nl}(S_p)n_0\mathcal{A}\left\{\, R_{Nl}(r)\left[Y_l(\hat{r})\left[\Phi^{j_1\pi_1}_{C_1}\Phi^{j_2\pi_2}_{C_2}\right]_{j_{12}}\right]_{JM}\right\},\end{aligned} \tag{B11}$$

in which the angular momenta of clusters are coupled to j_{12}, and j_{12} is coupled with the orbital angular momentum of the relative motion l yielding the total angular momentum J. $\Phi^{j_1\pi_1}_{C_1}$ and $\Phi^{j_2\pi_2}_{C_2}$ denote the projected internal wave functions, $\Phi^{j_1\pi_1}_{C_1} = \hat{P}^{j_1}_{m_1k_1}\Phi^{int}_{C_1}$ and $\Phi^{j_2\pi_2}_{C_2} = \hat{P}^{j_2}_{m_2k_2}\Phi^{int}_{C_2}$. When the inter-cluster distance S_p, $\quad p = 1, ..., p_{max}$ is dense discretized, and maximum (minimum) distance is chosen to be large (small) enough, a set of wave

functions given by Eq. (B11) should span the complete set for the $C_1 + C_2$ cluster states with above-mentioned angular momentum coupling, *i.e.*,

$$\sum_{pq} |\Phi^{J\pi}_{j_1\pi_1 j_2\pi_2 j_{12} l}(S_p)\rangle \, B^{-1}_{pq} \, \langle \Phi^{J\pi}_{j_1\pi_1 j_2\pi_2 j_{12} l}(S_q)| \simeq 1, \tag{B12}$$

$$B_{pq} = \langle \Phi^{J\pi}_{j_1\pi_1 j_2\pi_2 j_{12} l}(S_p) | \Phi^{J\pi}_{j_1\pi_1 j_2\pi_2 j_{12} l}(S_q)\rangle \, . \tag{B13}$$

Inserting Eq. (B12) into the definition of the RWA, we get

$$\begin{aligned} y^{J\pi}_{j_1\pi_1 j_2\pi_2 j_{12} l}(a) =& \sqrt{\frac{A!}{(1+\delta_{C_1C_2})C_1!C_2!}} \\ & \times \sum_{pq} \left\langle \frac{\delta(r-a)}{r^2} \left[Y_l(\hat{r}) \left[\Phi^{j_1\pi_1}_{C_1} \Phi^{j_2\pi_2}_{C_2} \right]_{j_{12}} \right]_{JM} \middle| \, \Phi^{J\pi}_{j_1\pi_1 j_2\pi_2 j_{12} l}(S_p) \right\rangle \\ & \times B^{-1}_{pq} \, \langle \Phi^{J\pi}_{j_1\pi_1 j_2\pi_2 j_{12} l}(S_q) | \Psi^{J\pi}_{MA} \rangle \, . \end{aligned} \tag{B14}$$

Using the completeness of the HO wave function $\sum_N R_{Nl}(r) R_{Nl}(a) = \delta(r-a)/r^2$ and Eq. (B11), the braket in the second line reads

$$\begin{aligned} & \left\langle \frac{\delta(r-a)}{r^2} \left[Y_l(\hat{r}) \left[\Phi^{j_1\pi_1}_{C_1} \Phi^{j_2\pi_2}_{C_2} \right]_{j_{12}} \right]_{JM} \middle| \, \Phi^{J\pi}_{j_1\pi_1 j_2\pi_2 j_{12} l}(S_p) \right\rangle = n_0 \sum_{NN'} a_{N'l}(S_p) R_{Nl}(a) \\ & \times \left\langle R_{Nl}(r) \left[Y_l(\hat{r}) \left[\Phi^{j_1\pi_1}_{C_1} \Phi^{j_2\pi_2}_{C_2} \right]_{j_{12}} \right]_{JM} \middle| \, \mathcal{A} \left\{ R_{N'l}(r) \left[Y_l(\hat{r}) \left[\Phi^{j_1\pi_1}_{C_1} \Phi^{j_2\pi_2}_{C_2} \right]_{j_{12}} \right]_{JM} \right\} \right\rangle \\ & = n_0 \sum_N a_{Nl}(S_p) \mu_{Nl} R_{Nl}(a). \end{aligned} \tag{B15}$$

In the last line, we assumed that $\Phi^{j_1}_{C_1}$ and $\Phi^{j_2}_{C_2}$ are eigenstates of the principal quantum number $\hat{N}$. In this case, the braket in the second line is non-zero only when $N = N'$, and we denote it $\mu_N \delta_{NN'}$. From Eqs. (B14) and (B15), we get

$$y^{J\pi}_{j_1\pi_1 j_2\pi_2 j_{12} l}(a) = \frac{1}{\sqrt{1+\delta_{C_1C_2}}} \sum_N \mu_{Nl} \left(\sum_{pq} a_{Nl}(S_p) B^{-1}_{pq} \, \langle \Phi^{J\pi}_{j_1\pi_1 j_2\pi_2 j_{12} l}(S_q) | \Psi^{J\pi}_{MA} \rangle \right) R_{Nl}(a). \tag{B16}$$

Simplifying this equation, we obtain Eqs. (43), (44), (45) and (46).